UCRL-ID-121414

PCMDI
Program for Climate Model Diagnosis and Intercomparison

PCMDI Report No. 22

THE EFFECT OF HORIZONTAL RESOLUTION ON CLOUD RADIATIVE FORCING IN THE ECMWF MODEL

by

Gerald L. Potter

Program for Climate Model Diagnosis and Intercomparison
Lawrence Livermore National Laboratory, Livermore, CA, USA

May 1995

PROGRAM FOR CLIMATE MODEL DIAGNOSIS AND INTERCOMPARISON
UNIVERSITY OF CALIFORNIA, LAWRENCE LIVERMORE NATIONAL LABORATORY
LIVERMORE, CA 94550

DISCLAIMER

This document was prepared as an account of work sponsored by an agency of the United States Government. Neither the United States Government nor the University of California nor any of their employees, makes any warranty, express or implied, or assumes any legal liability or responsibility for the accuracy, completeness, or usefulness of any information, apparatus, product, or process disclosed, or represents that its use would not infringe privately owned rights. Reference herein to any specific commercial product, process, or service by trade name, trademark, manufacturer, or otherwise, does not necessarily constitute or imply its endorsement, recommendation, or favoring by the United States Government or the University of California. The views and opinions of authors expressed herein do not necessarily state or reflect those of the United States Government or the University of California, and shall not be used for advertising or product endorsement purposes.

This report has been reproduced
directly from the best available copy.

Available to DOE and DOE contractors from the
Office of Scientific and Technical Information
P.O. Box 62, Oak Ridge, TN 37831
Prices available from (615) 576-8401, FTS 626-8401

Available to the public from the
National Technical Information Service
U.S. Department of Commerce
5285 Port Royal Rd.,
Springfield, VA 22161

Abstract

The ECMWF general circulation model was (cycle 33) used to test the effect of horizontal resolution on the simulated cloud radiative forcing. The model was run with four resolutions: T21, T42, T63 and T106 and the results were compared to the Earth Radiation Budget Experiment (ERBE). The ECMWF model produces relatively large errors in comparison to observations for January and July which can be attributed to the model being too dry and clouds too reflective. Only the T21 resolution displays substantial differences from the other resolutions, and all resolutions are substantially different from observations from ERBE.

1. Introduction

With expanding computer capability and capacity there has been considerable interest in increasing the resolution in GCMs. The primary driving force behind this are two fold: 1) increased resolution may reduce the systematic errors inherent in parameterization of sub-grid scale processes, and 2) higher resolution may improve confidence in regional scale studies of climatic features that are orographically influenced - such as the effect of the Tibetan Plateau on the East Asian Monsoon (Sperber et al., 1993). This study focuses on the effect of horizontal resolution on the spatial and temporal systematic errors of cloud radiative forcing and its components. Previous resolution studies such as those by Mahlman and Umscheid (1987), Boer and Lazare (1988), Rind (1988), Tibaldi et al. (1990), Boville (1991), Kiehl and Williamson (1991) and Boyle (1993) have been concerned with the effects of varying horizontal and vertical resolution. The ECMWF model performance as reported by Boyle (1993) was not enhanced with higher resolution and in fact, some of the general characteristics of that model were degraded in the higher resolutions compared to the coarsest resolution (Phillips et al., 1993).

In this paper, the top-of-the-atmosphere radiation fields are taken from a series of simulations using the European Centre for Medium Range Forecasts (ECMWF) general circulation model (cycle 33), run at four different horizontal resolutions. Section 2 discusses the concept of cloud radiative forcing and describes the simulations from the ECMWF model. The observed global field of cloud forcing from ERBE is presented in section 3 along with the model-produced fields of the net solar and longwave cloud forcing. The seasonal effect of forcing is described in section 4, and the results are summarized in section 5.

2. Methodology

2.1 The ECMWF model cycle 33

The ECMWF general circulation model used in these simulations is described in Simmons et al. (1988) and Tiedtke et al. (1988). The model includes the diurnal cycle of insolation. The physical tendencies are calculated on a Gaussian grid where the grid sizes (deg lat) for the resolutions are 1.125 at T106, 1.875 at T63, 2.8125 at T42 and 5.625 at T21. The model was integrated for one year at each resolution and an additional six months for the T42 and T106 resolutions. While it is recognized that these simulations are too short to make definitive statements, the purpose of the paper is to provide a general view of the model's systematic errors in the cloud radiative forcing.

2.2 Cloud radiative forcing

The concept of cloud radiative forcing has been used to explore the effect clouds have on the top-of-the-atmosphere energy balance. The net cloud radiative forcing is defined as the difference between the total long and short wave fluxes at the top of the atmosphere (total) and that of the respective clear sky fluxes (clear), that is

$$CRF_{net} = F_{clear} - F_{total} - Q_{clear} + Q_{total} \ .$$

where F and Q are respectively the net upward infrared and net downward solar fluxes. The concept is useful because it allows comparison of the radiative impact of clouds without requiring knowledge of cloud height or cloud cover.

One difficulty in comparison with observational data stems from the determination of F_{clear} and Q_{clear} as was discussed in Potter el al. (1992). Of the several methods available we determined that Method II was appropriate for this study. Direct comparison with the Earth Radiation Budget Experiment (ERBE; Barkstrom, 1984 and Harrison et al., 1990) reveals large systematic errors well beyond the relatively small differences among the different resolutions of the model. This method uses the radiation calculation for total fluxes at the top of the atmosphere but with the clouds removed. By employing this method the flux is available at every space and time point. The time-averaged clear sky flux at a grid point is given by where F_i^{clear} is the clear sky flux computed by the model and N is the total number of samples (the total number of radiation time steps).

3. Cloud Radiative Forcing Results

3.1 Longwave cloud radiative forcing

One of the difficulties in validating cloud radiative forcing is that the available ERBE data cover only 4 years. As a result of the interannual variability inherent in ERBE, large regional variations exist from year to year. This variability as shown below is well below the systematic differences between ERBE and the model-produced fields of cloud radiative forcing. Figure 1 shows the global distribution of the average July longwave cloud radiative forcing from ERBE (CRF_{lw}) and the July CRF_{lw} for the years 1985, 1986, 1987 and 1988. The largest differences occur in areas of tropical convergence in the western Pacific between 1987 and the other years. Generally, the pattern of interannual variability is similar for the other months and for CRF_{sw}. In general, the large scale regional observed CRF_{lw} is dominated in July by peak values over the northern tropical oceans (Harrison et al., 1990) where the deep convective clouds with their associated high cold tops reduce the outgoing flux of LW radiation. This in turn results in a high positive cloud forcing in comparison with the clear skies. The extratropical storm tracks are also typified by rel-

atively high values CRF_{lw}. Lower values of CRF_{lw} result from lower, warmer clouds or lack of significant cloud cover. High values of CRF_{lw} also occur over warm water flowing under relatively cold air such as over the Gulf Stream and to a lesser extent over the Kiroshiro current. The January CRF_{lw} also highlights the South Pacific Convergence Zone as a region of extensive cloud cover resulting in enhanced CRF_{lw} (not shown). Another region of presumably high CRF_{lw} in July is over central South America. The amount of missing data here results from ERBE's inability to "see" any clear sky is significant, and is testimony to the cloudiness that persists over the tropical land surfaces during the high sun period.

Figure 2 shows results from ERBE for the year 1987 and the subsequent Figs. 3-6 show the four resolutions (T21, T42, T63 and T106 respectively) of the ECMWF model for January and July. A distinguishing feature of all model resolutions is the very high values of CRF_{lw} over the tropical oceans. This results from the systematic dry bias in the ECMWF Cy33 (Phillips et al., 1993). This strong positive CRF_{lw} is often attributed to persistent deep clouds, but in this case it is likely a consequence of excessive outgoing longwave radiation regardless of clouds. As can be seen from the zonal averaged clear sky flux (Fig. 3), all model resolutions exceed the average ERBE clear sky flux by as much as 20 Wm^{-2}. This, in conjunction with the very intense, concentrated ITCZ, contributes to the higher than observed values. The model does, however, produce results similar to ERBE over the southern Indian Ocean and over the area of the Indian Monsoon (see also Sperber et al., 1994). There is also some indication of the southwestern North American Monsoon which does not appear in the ERBE data. This is likely due to the short period of sampling from both ERBE and the single year of integration of the model.

Another systematic error occurs over the eastern margins of the subtropical oceans. The ECMWF model tends to underpredict the stratus cloud decks common in these regions and consequently the outgoing radiation freely passes to space. Although these low clouds have much the same outgoing longwave radiation as the surface, the ECMWF cycle 33 model is also considerably drier than observed (Phillips et al., 1993). Nearly all of the spatial patterns are maintained at T42, T63 and T106 resolutions, and it is in fact difficult to distinguish between the T63 and T106 resolutions.

The T21 simulation is somewhat different than the higher resolution cases, particularly in the Western Pacific where the higher resolutions produce a double ITCZ. This feature is most prominent in the Indian Ocean and South East Asia. In part, this is the result of low evaporative fluxes in conditions of low wind speed. An engineering fix to this model feature was one of the major modifications in a later version of the ECMWF model. It is interesting to note that the lowest resolution (T21) produces more realistic CRF_{lw} than the higher resolutions, probably due to the coarseness of the resolution and its inability to resolve the erroneous double ITCZ.

In January (Figs. 4a, 5a, 6a, and 7a), one feature that is very obvious is the lack of the southern excursion of the ITCZ in the South Pacific Ocean. This version of the ECMWF model also lacks a general organization of the South Pacific Convergence Zone and the low values of CRF_{lw} over the eastern South Pacific produce the same features as ERBE. Over Africa the T21 resolution appears to produce poor results while the higher resolution models are more realistic.

3.2 Shortwave cloud radiative forcing

Figure 2d shows the July CRF_{sw} for ERBE, and the corresponding four resolutions of the ECMWF model are shown in Figs 4d, 5d, 6d, and 7d. The primary difference between all resolutions of the model and ERBE is the model's tendency to produce too large (negative) CRF_{sw} over active convective regions. This is particularly apparent over the oceans, and is largely due to the scattering introduced by a parametrization in cloud liquid water making the clouds generally too bright. As a result, the ECMWF model clouds have high negative CRF_{sw}. The errors produced by this particular parameterization are apparent in the seasonal response as well as in individual months. It is noteworthy that although the CRF_{sw} exhibits such a large systematic error, it has very little to do with the general performance of the model. The diabatic heating of the atmosphere is relatively uninfluenced by the erroneous solar cooling by CRF_{sw} over the oceans because the ocean temperatures are fixed. Generally, values of CRF_{sw} show most similarity to observations over land, particularly in the subtropics.

The CRF_{sw} for the month of January is shown in Figs. 4b, 5b, 6b, and 7b. The summer hemisphere is subject to many of the same errors as in July, although one interesting feature is the winter monsoon over East Asia where the polar front appears in all resolutions. The model does not, however, produce the band of minimum CRF_{sw} detected by ERBE across Europe and Central Asia.

3.3 Net cloud radiative forcing

The global distribution of July net cloud radiative forcing (CRF_{net}) for ERBE is shown in Figure 8a and can be compared with the four model resolutions for July in Figs. 9b, 10b, 11b, and 12b. These figures show large systematic errors between the model and ERBE and relatively small differences among the different model resolutions. One of the dominant features from ERBE is the area of large negative CRF_{net} in the midlatitude storm tracks in the summer hemisphere. It is here that the CRF_{sw} outweighs the CRF_{lw} because the solar input is at a maximum in the summer hemisphere. Conversely, the largest positive area of CRF_{net} is over the midlatitude storm tracks in the winter hemisphere where the sun angle is low and the heating from CRF_{lw}

dominates (positive values). In many regions CRF_{net} shows the balancing of CRF_{sw} and CRF_{lw} and is near zero. Figure 13 shows the global values of CRF_{lw}, CRF_{sw}, and CRF_{net} for ERBE and the four resolutions of the ECMWF model. From these global values for January and July the most obvious error in all resolutions is the excessively negative CRF_{sw}, and is due to the highly reflective clouds. This same feature was responsible for the negative cloud feedback in the ± 2K SST perturbation study of Cess et al. (1989).

4. Seasonal Cloud Forcing

Cess et al. (1992) point out that it is impossible to determine cloud feedback from a seasonal model run using the seasonal excursion of cloud forcing as a surrogate for a climate change. They do, however, offer a method of calculating a measure of the seasonal ΔCRF that gives an indication of the contribution of cloud forcing for January and July in comparison with the annual average. This measure of the seasonal cycle of CRF_{lw} and CRF_{sw} provides a method of isolating the systematic errors of cloud height and cloud radiative properties. Following Cess et al. (1992)

$$\Delta CRF = S(\Delta\alpha_c - \Delta\alpha) + (\Delta F_c - \Delta F)$$

where Δ is the seasonal perturbation of a quantity about the annual mean and where ΔF and Δα represent the monthly-mean departures from the annual mean, c is the clear-sky component, and S is the monthly-mean solar irradiance. If ΔCRF were a measure of the change in cloud forcing for the entire globe, then it could be interpreted as cloud feedback (Cess el al., 1989, 1990). However, it is largely the seasonal variation of the ITCZ that dominates ΔCRF caused by changes in cloud cover, cloud optical properties, cloud height, and solar zenith angle.

4.1 Zonal average ΔCRF

The seasonal contribution of CRF_{lw} to the annual mean (ΔCRF_{lw}) is negatively correlated with ΔCRF_{sw} as seen in Figures 14a and 14b compared to the Figures 14c and 14d. The ERBE data in these figures clearly demonstrate this feature. In January, areas with large positive ΔCRF_{lw} denote intense convective regions where the effect of the deep convective cloud compared to the annual mean is at a maximum. Conversely, in July the maximum radiative warming compare to the annual mean occurs in the Northern Hemisphere collocated with the maximum of the ITCZ. The ECMWF model produces a much more believable ΔCRF_{lw} than ΔCRF_{sw} and is more consistent among the different resolutions. This correspondence between the model and ERBE for ΔCRF_{lw} is largely due to the seasonally varying prescribed sea surface temperatures and the associated

enhanced outgoing longwave radiation. The systematically dry model atmosphere enhances the impact of clouds and the effect of January or July compared to the seasonal mean.

The January zonal averaged values of ΔCRF_{sw} for ERBE and the four resolutions are shown in Figure 14b. The ERBE ΔCRF_{sw} data are dominated by the seasonal excursion of the ITCZ, where the shortwave response of clouds (CRF_{sw}) in January compared to the annual average is to cool the atmosphere where the clouds are very bright (intense convection). Heating from ΔCRF_{sw} compared to the annual average occurs where the storm tracks move poleward. The July ΔCRF_{sw} (Figure 12d) is negatively correlated with that in January, and shows that the northern hemisphere CRF_{sw} in July compared to the annual mean is larger than the southern hemisphere CRF_{sw} in January. ΔCRF_{sw} cools where convection is the strongest and acts as a "negative feedback" in those areas of intense convection. The relative warming of the summer hemisphere seen in the mid-latitudes compared to the annual cycle is a result of the storm belts moving poleward in the summer hemisphere, although this feature is less pronounced in the Southern Hemisphere. The ECMWF model maintains the general character of the ΔCRF_{sw} but the tropical cooling is displaced approximately 10 degrees of latitude poleward. All of the ECMWF model resolutions show in this error, which is connected to the position of the ITCZ which, in this particular version of the model, produces a double convective maximum in all but the T21 resolution. The principal reason for this systematic error is the poleward displacement of the summer hemisphere ITCZ. The data show a double simulated ITCZ, with one center at 5 N and another at 25 N in July, with a similar error in January with the primary peak more diffuse among the resolutions, and the secondary peak less pronounced and closer to the equator in than in July. The T21 resolution does not appear to resolve the double ITCZ in ΔCRF_{sw} in either season and consequently looks somewhat more realistic. The possibility that the lower resolutions may produce better tropical convection has been pointed out by J. M. Slingo (personal communication, 1994).

In general, the zonal averaged features of ΔCRF_{lw} and ΔCRF_{sw} suggest that the ECMWF model contains structure in the seasonal forcing that does not appear in the observations. This structure, caused by a split in the ITCZ, is less pronounced in the lower resolutions and disappears entirely in the T21 resolution. The effect of seasonal cloud forcing in the tropics is shifted to higher than observed latitudes at all resolutions. The general structure of ΔCRF_{lw} is closer to observations than ΔCRF_{sw} (Figs. 14a and 14b vs. 14c and 14d) in all resolutions, but there is very little improvement with increased resolution.

4.2 Global distribution of ΔCRF

The global distribution of ΔCRF is shown for both LW and SW for January and July 1988 in Figure 15. The dominant features of the observed flux are the large differences between the January and July ΔCRF. As pointed out by Cess et al. (1992), one prominent feature of the ΔCRF in July is the strong positive SW ΔCRF and the somewhat smaller negative LW ΔCRF in the north Atlantic. The seasonal response in this case is dominated by the enhanced cloud cover in winter. Strong positive ΔCRF_{sw} in July suggests relatively clear sky compared to the annual mean, and negative ΔCRF_{lw} in July suggests drier conditions than the annual average atmosphere that corresponds with clear skies. It is interesting to note that Cess et al. (1992), using a different ERBE year data (1985), in the area of the East Asian Monsoon find that ΔCRF_{sw} and ΔCRF_{lw} are both positive. This feature was explained from the differing cloud heights in July compared to the annual average. In the case of other ERBE periods, there is significant interannual variability in the ERBE data due to cloud height and depth changes in the monsoon area.

The T21 resolution (Fig. 16) shows the ΔCRF for both LW and SW to have somewhat exaggerated values. Although the pattern of ΔCRF has some of the same features as ERBE, the intensity of the positive LW cloud forcing compared to the annual average over the Indian Monsoon is much too intense and covers considerably larger areas than observed. The positive ΔCRF_{sw} in the northern Atlantic and the corresponding negative ΔCRF_{lw} are not reproduced as well in the T21 resolution as in the higher resolutions (Figs. 17-19). This contradicts the performance of the T21 model for CRF (Fig. 3) where the lowest resolution appears to produce slightly more realistic features as seen in the ITCZ in January and July. All resolutions of the model produce a confused annual cycle in the Pacific Basin. This can be attributed partly to the double ITCZ but also to the general dryness and the lack of well defined storm paths in the north Pacific. The July values of ΔCRF_{sw} and ΔCRF_{lw} suggest that the cloud systems associated with extratropical cyclones are too far north. Again in the north Pacific the higher resolutions seem to depict more of the seasonal cycle. In general, all resolutions appear to exaggerate the summer hemisphere contribution to the seasonal cycle compared to ERBE.

5. Conclusions

In general, increasing horizontal resolution from T21 to T106 had little or no effect on the systematic errors of cloud radiative forcing produced by the ECMWF Cy33 model. This is in general agreement with the results of Boyle (1994) and Phillips (1994).

Two compensating errors in the model cloud radiative forcing are dominant in the comparison with observations. The ECMWF model is consistently too dry which results in anomalously high values of CRF_{lw}. Zonally averaged, the CRF_{lw} is as much as 20 Wm^{-2} too high in most latitudes. The CRF_{sw} is also too negative because of the highly reflective convective clouds. One might expect the net cloud forcing to be closer to reality because of these compensating errors, but the negative CRF_{sw} bias dominates the model and the CRF_{net} is generally too negative.

There is some indication that the seasonal cycle of CRF does improve somewhat at T42 and higher resolutions, leaving the T21 resolution as an outlier. The T21 resolution produces a slightly more believable CRF in the tropics, related to the inability to resolve the double ITCZ that is characteristic of cycle 33. Overall, the model produces some of the large scale features of the seasonal cycle as defined by ΔCRF. This is encouraging because if ΔCRF_{lw} and ΔCRF_{sw} are realistic the cloud response to climate change also has increased credibility.

Problems in validating model cloud forcing arise from how to use the available ERBE data and how to best mimic the retrieval method used to process the ERBE data. It was decided that the best use of ERBE was to evaluate the different years of ERBE and to identify robust large scale patterns. Averaging the monthly fluxes for four years gives some indication of the large scale patterns, but difficulties arise as to interpretation of the locations and significance of areas with persistent missing clear sky data (i.e., the satellite inability to detect any clear sky pixels for an entire month). It was also determined that for the purposes of this paper, using 1988 or 1987 data was acceptable since the average global difference between model and ERBE is on the order of 20-50 Wm-2 while the interannual variability of ERBE is globally 2-3 Wm^{-2} (Vonder Haar and Randel, 1994).

Acknowledgments

I gratefully acknowledge the ECMWF for making the forecast model available for this research. The simulations were performed at the National Energy Research Supercomputer Center. This work was supported by the Environmental Sciences Division, Office of Energy Research, U. S. Department of Energy and performed by the Lawrence Livermore National Laboratory under U. S. Department of Energy Contract W-7405-Eng-48 with the University of California.

References

Barkstrom, B. R., 1984: The Earth Radiation Budget Experiment (ERBE), Bull. Am. Meteor. Soc., 65, 1170-1185.

Boer, G. J., and M. Lazare, 1988: Some results concerning the effect of horizontal resolution and gravity-wave drag on simulated climate. J. Clim., 1,798-806.

Boville, B. A., 1991: Sensitivity of simulated climate to model resolution., J. Clim., 1 796-806.

Boyle, J. S., 1992: Sensitivity of dynamical quantities to horizontal resolution for a climate simulation using the ECMWF (cycle 33) model. J. Clim., 1, 789-806.

Cess R. D., E. F. Harrison, P. Minnis, B. R. Barkstrom, V. Ramanathan and T. Y. Kwon, 1992: Interpretation of seasonal cloud-climate interactions using Earth radiation budget experiment data. J. Geophys. Res. D7, 7613-7617.

Harrison, E., F. P. Minnis, B. R. Barkstrom, V. Ramanathan, R. D. Cess and G. G. Gibbson, 1990: Seasonal variation of cloud radiative forcing derived from the Earth Radiation Budget Experiment, J. Geophys. Res. D11, 18,867-18,703.

Kiehl, J. T., and D. L. Williamson, 1991: Dependence of cloud amount on horizontal resolution in the National Center for Atmospheric Research Community Climate Model. J. Geophys. Res., 96D, 10,955-10,980.

Mahlman, J. D., and L. J. Umscheid, 1987: Comprehensive modeling of the middle atmosphere: The influence of horizontal resolution. In Transport Processes in the Middle Atmosphere, G. Visconti and R. Garcia (eds), Reidel, Amsterdam, 251-266.

Sperber, K. R., S. Hameed, G. L. Potter and J. S. Boyle, 1994: Simulation of the Indian and East-Asian summer monsoon in the ECMWF model: sensitivity to horizontal resolution. *Mon. Wea. Rev.*, 122, 2461-2481.

Phillips, T. J., L. C. Corsetti and S. L. Grotch, 1994: The impact of horizontal resolution on moist processes in the ECMWF model. UCRL-ID-112719, PCMDI Report No. 8, Clim. Dyn, 11, 85-102.

Potter, G. L., J. M. Slingo, J-J. Morcrette and L. Corsetti, 1992: A modeling perspective on cloud radiative forcing. J. Geophys. Res, D18, 20507-20-518.

Rind, D., 1988: Dependence of warm and cold climate depiction on climate model resolution. J. Clim., 1, 965-997.

Tibaldi, S., T. N. Palmer, C. Brankovic and U. Cubasch, 1990: Extended-range predictions with ECMWF models: Influence of horizontal resolution on systematic error and forecast skill. Quart. J. Roy. Meteor. Soc., 116, 835-866.

Vonder Haar, T. H., and D. L. Randel, 1994: The natural variability of cloud forcing, Preprints AMS Seventh Conference on Satellite Meteorology and Oceanography, June 6-10, 1994, Monterey, CA.

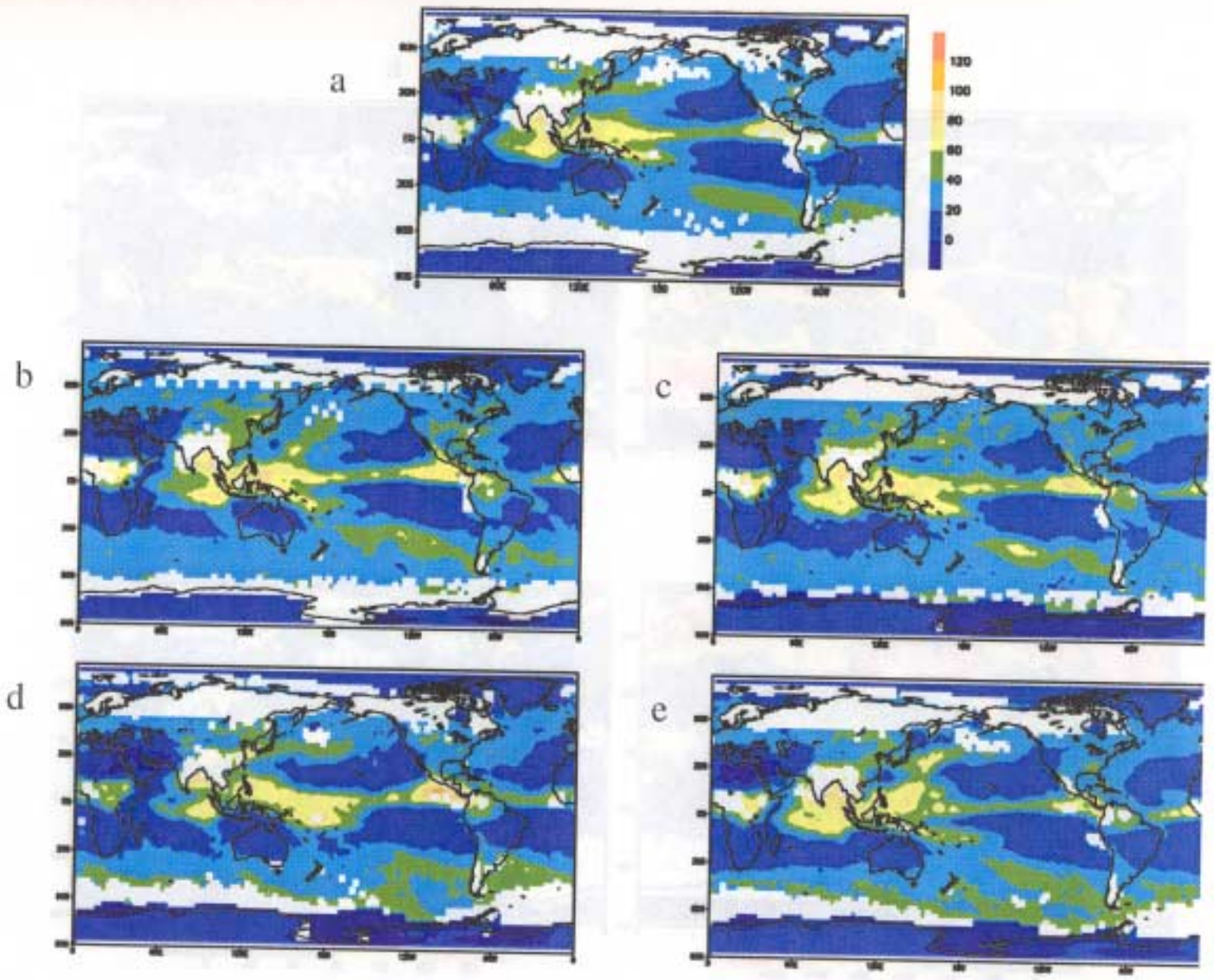

Figure 1. The ERBE July averaged longwave cloud radiative forcing (CRF_{lw}) in Wm^{-2} for: a) 4 year average (1985-1988), b) 1985, c) 1986, d) 1987 and e) 1988.

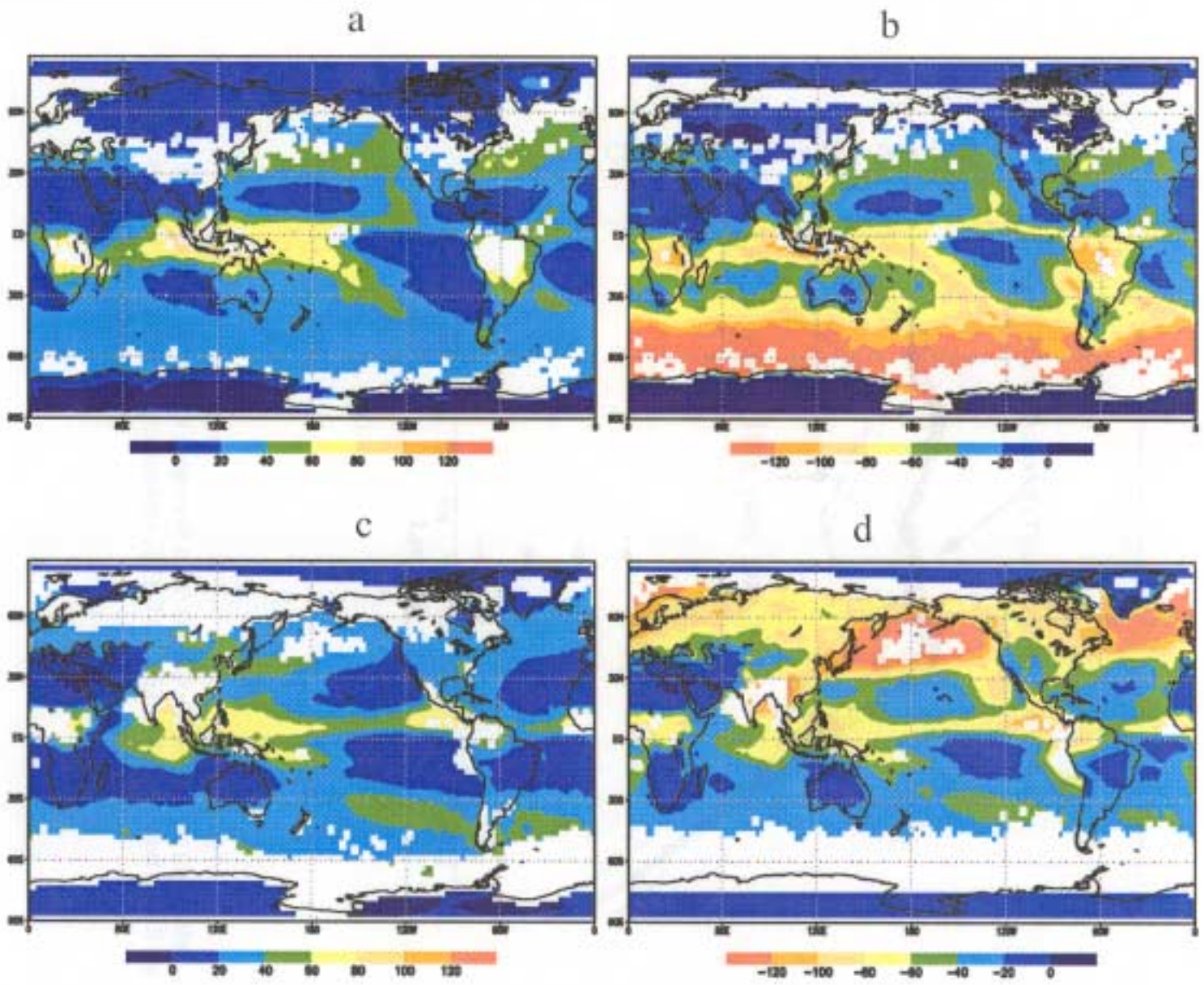

Figure 2. The ERBE 1988 cloud radiative forcing in Wm^{-2} for: a) January CRF_{lw}, b) January CRF_{sw}, c) July CRF_{lw} and d) July CRF_{sw}.

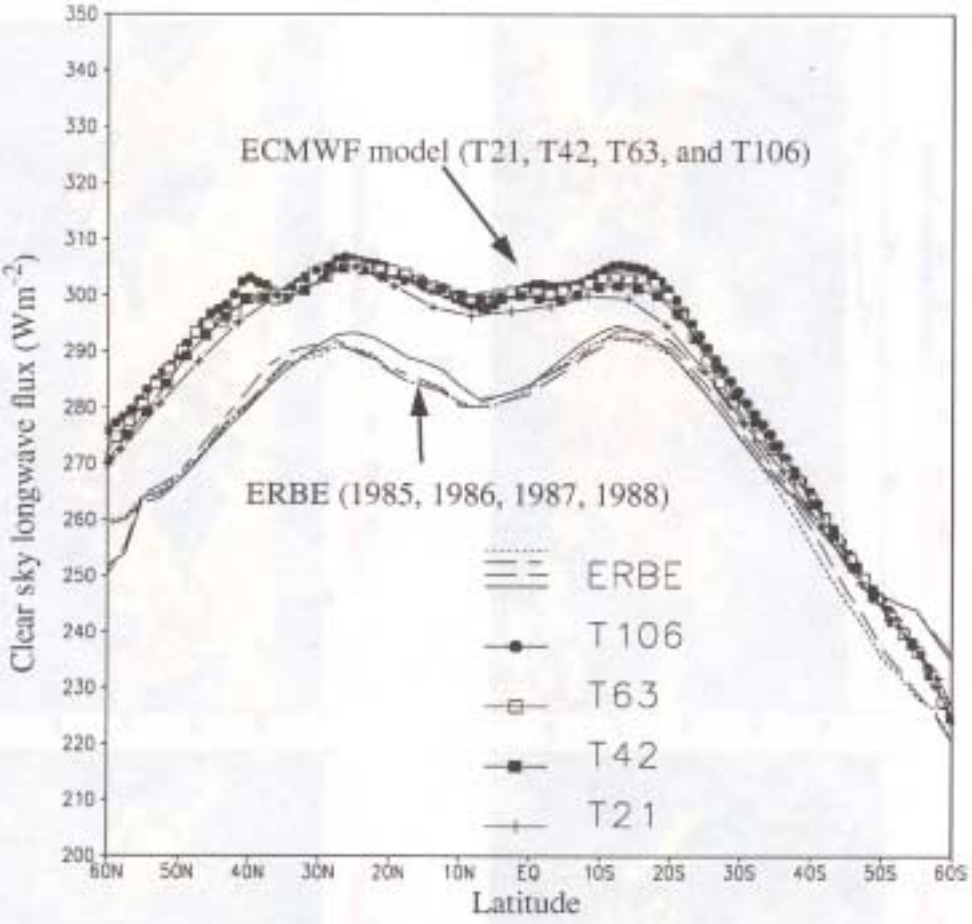

Figure 3. July zonal average of longwave clear-sky flux (Wm^{-2}) at the top of the atmosphere for the four model resolutions (T21, T42, T63, and T106) and ERBE for 1985, 1986, 1987, and 1988.

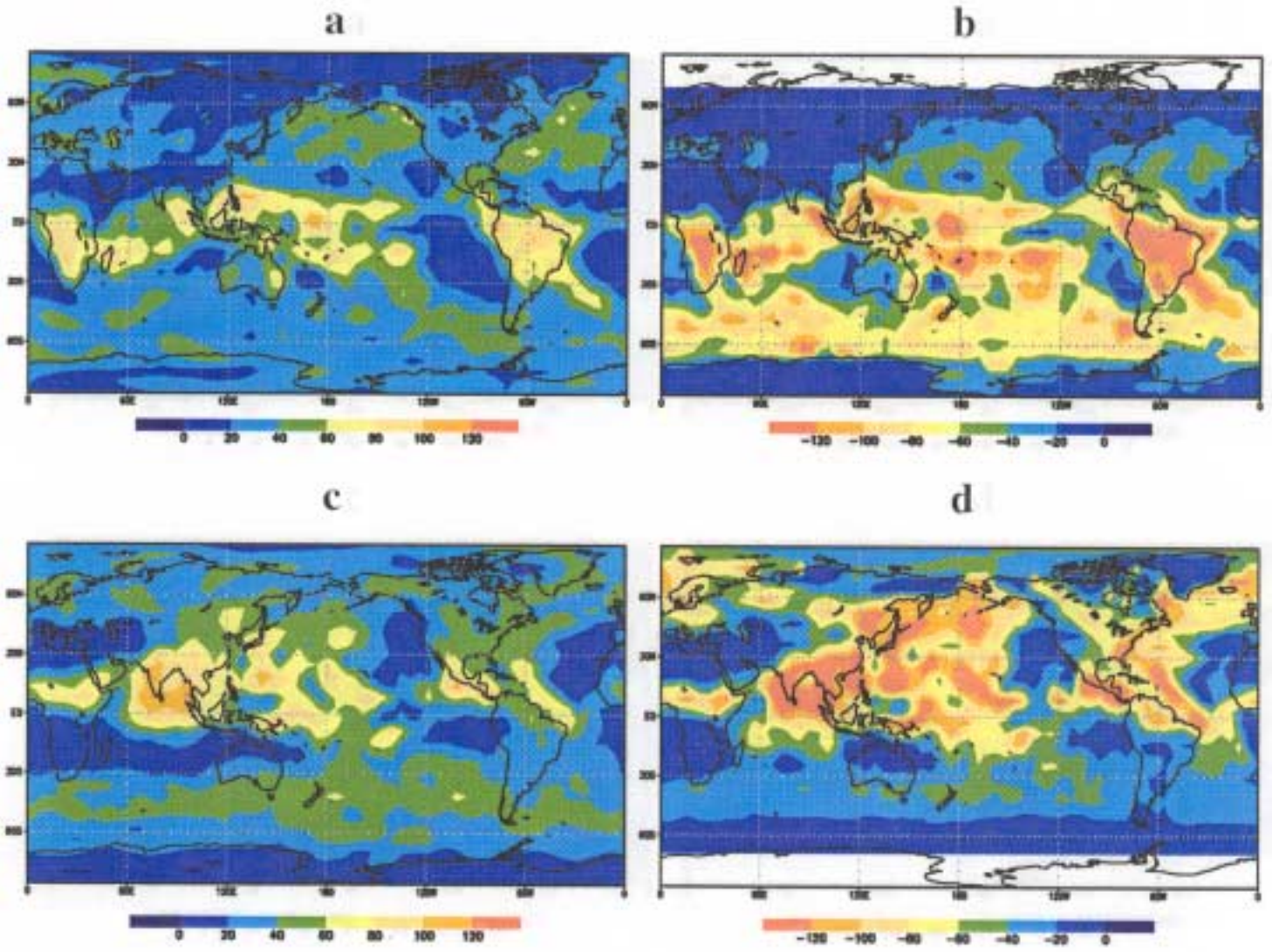

Figure 4. The ECMWF T21 resolution CRF in Wm-2 for: a) January CRF_{lw}, b) January CRF_{sw}, c) July CRF_{lw}, and d) July CRF_{sw}.

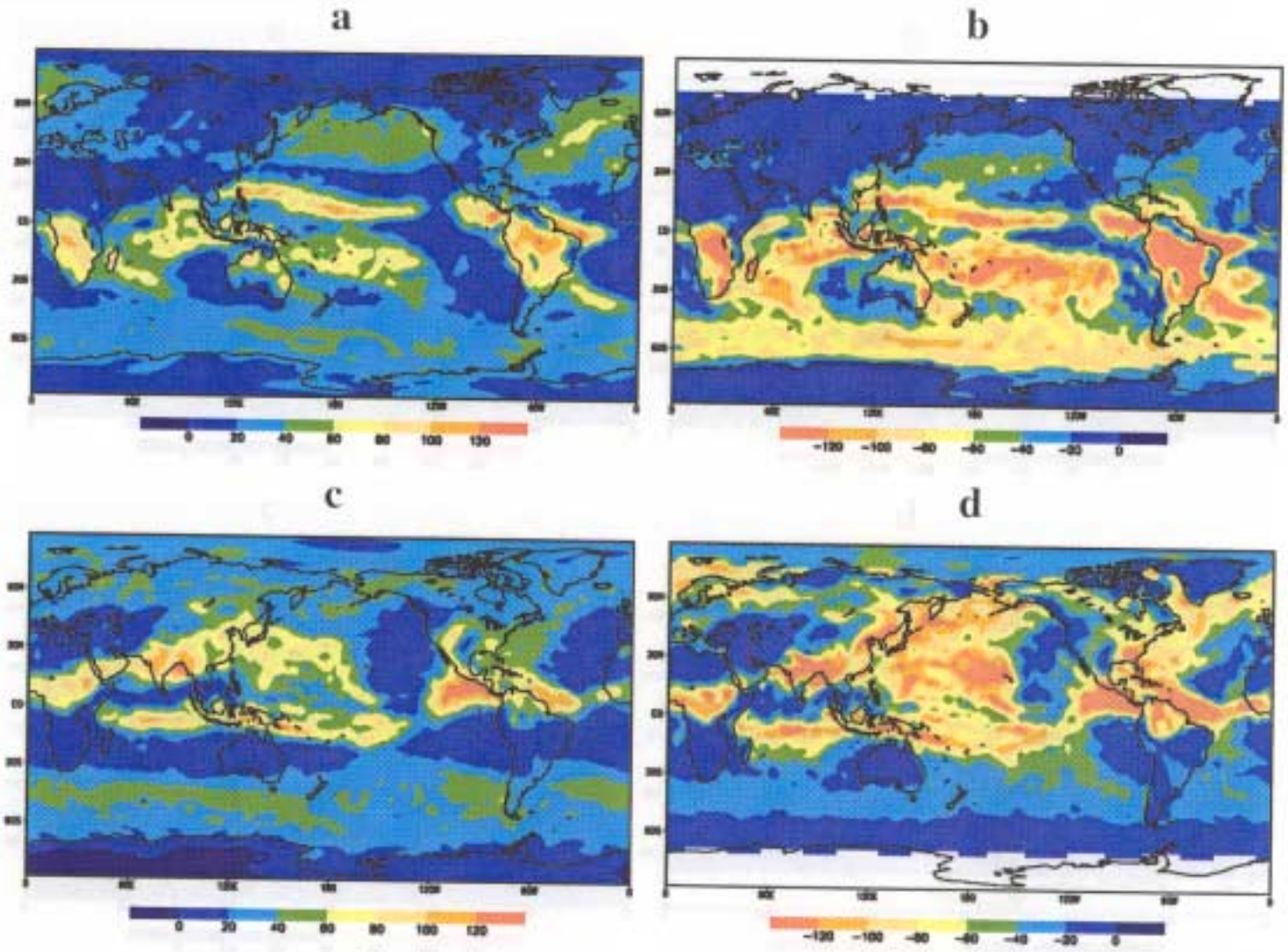

Figure 5. The ECMWF T42 resolution as in Figure 4.

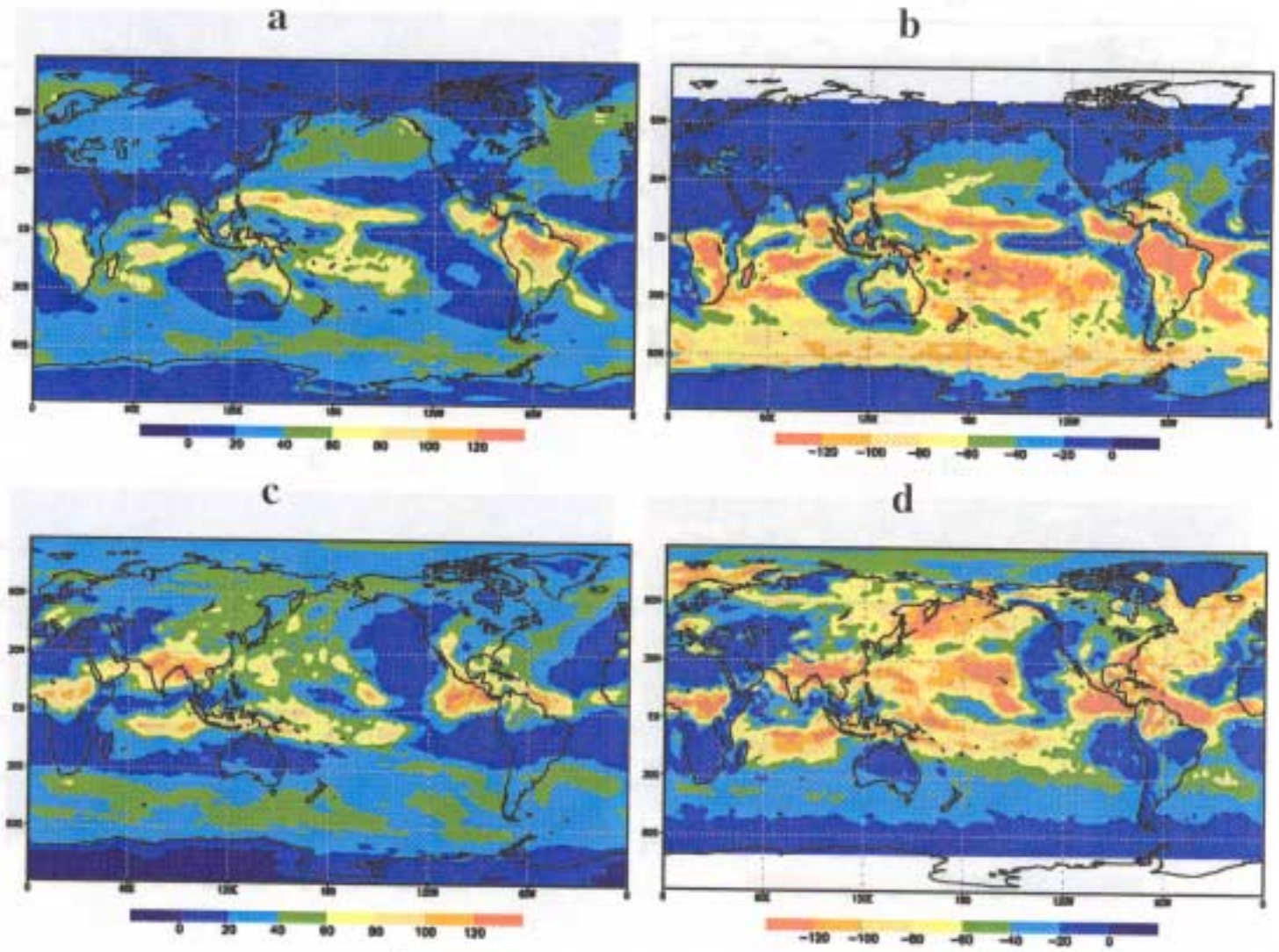

Figure 6. The ECMWF T63 resolution as in Figure 4.

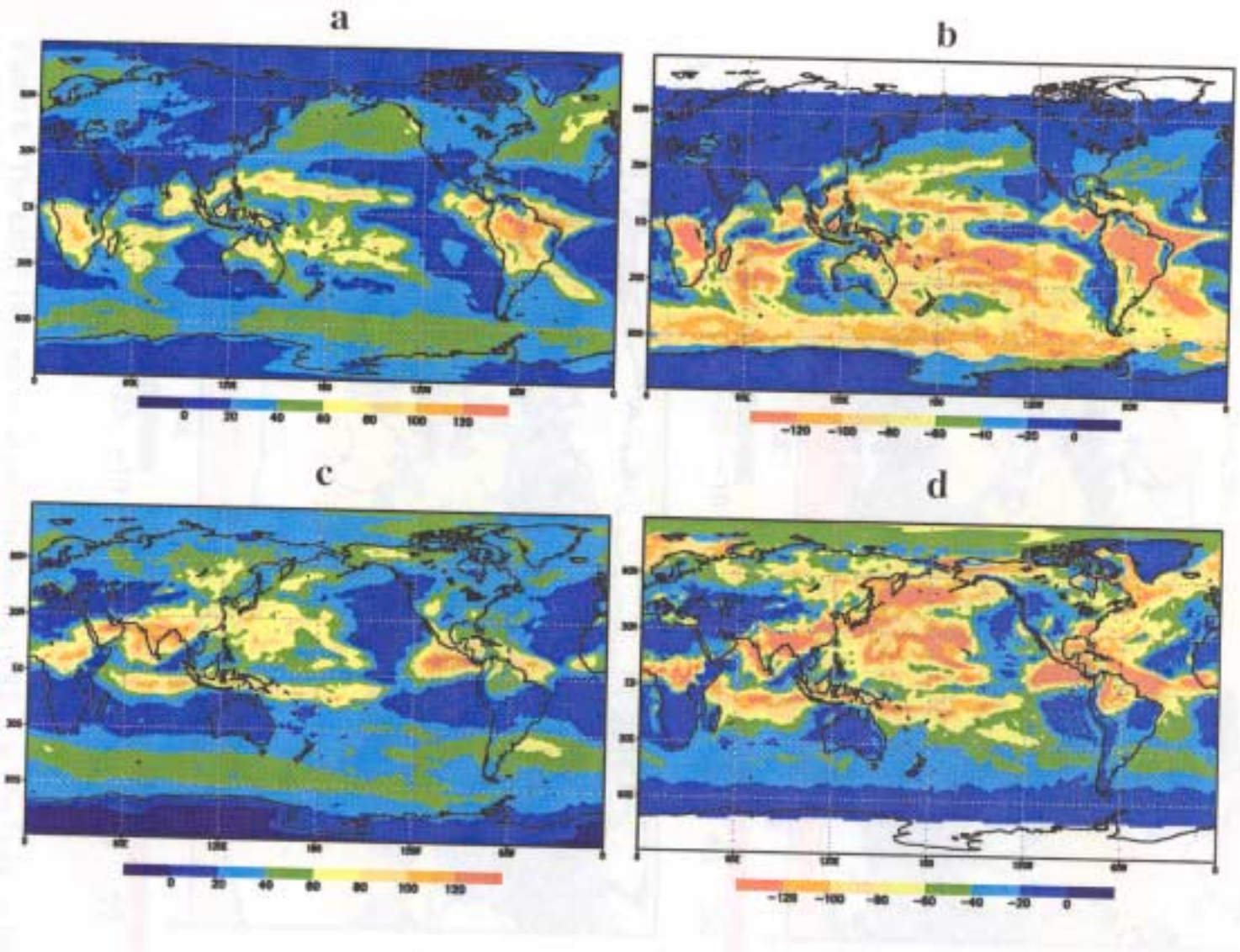

Figure 7. The ECMWF T06 resolution as in Figure 4.

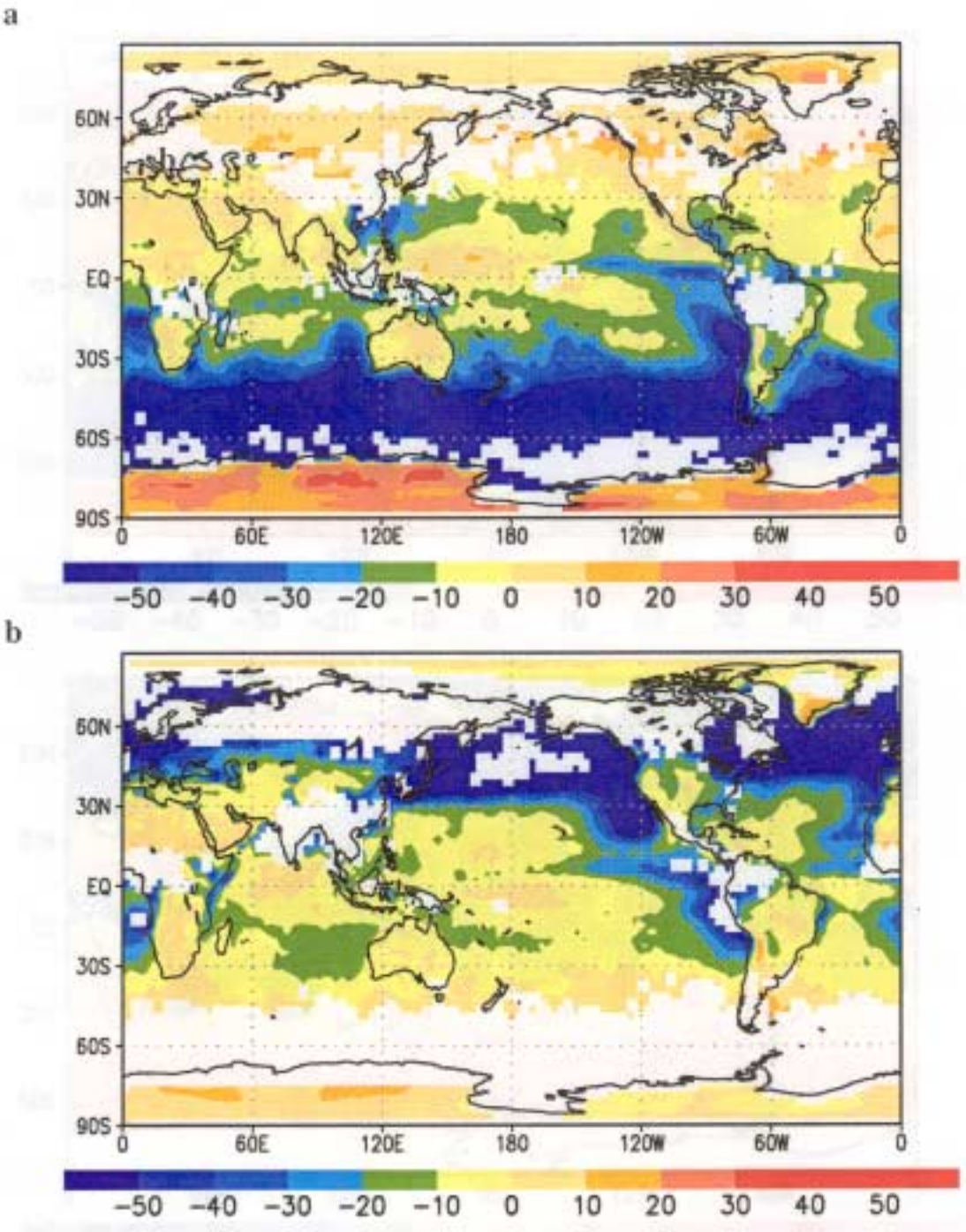

Figure 8. The ERBE 1988 net cloud radiative forcing (CRF_{net} in Wm^{-2}) for: a) January, and b) July.

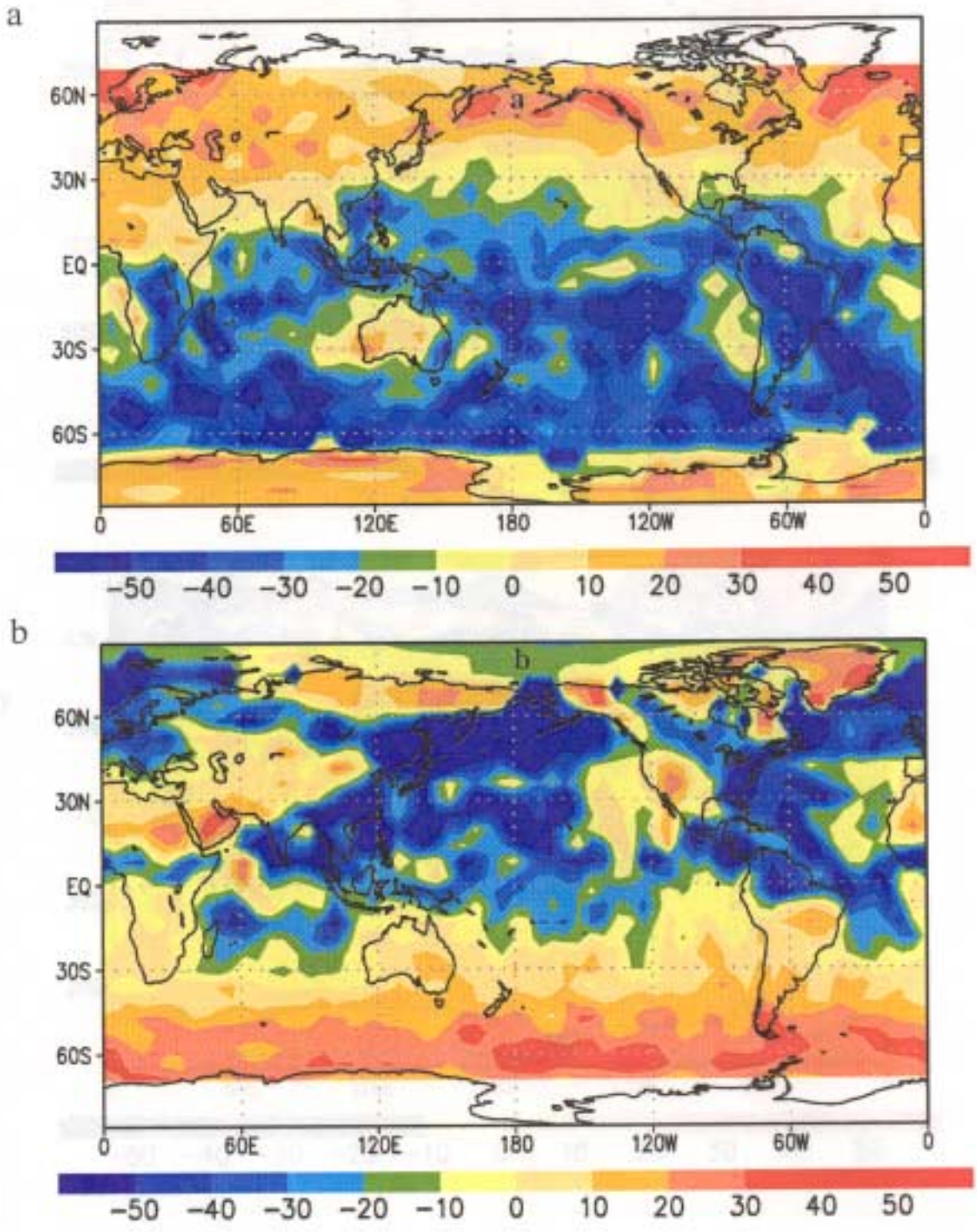

Figure 9. The ECMWF T21 net cloud radiative forcing (CRF_{net} in Wm^{-2}) for: a) January, and b) July.

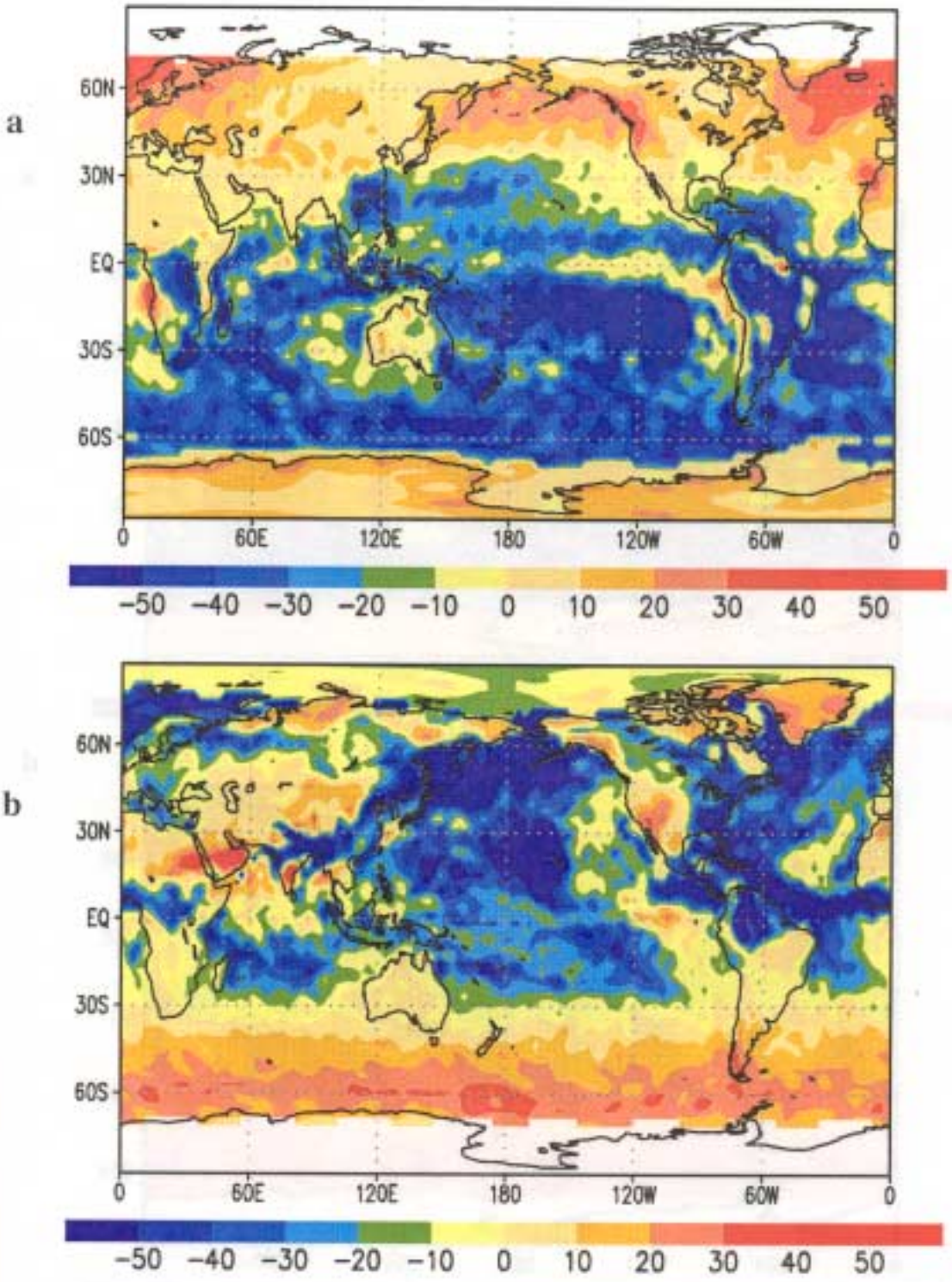

Figure 10. The ECMWF T42 net cloud radiative forcing (CRF_{net} in Wm^{-2}) for: a) January, and b) July.

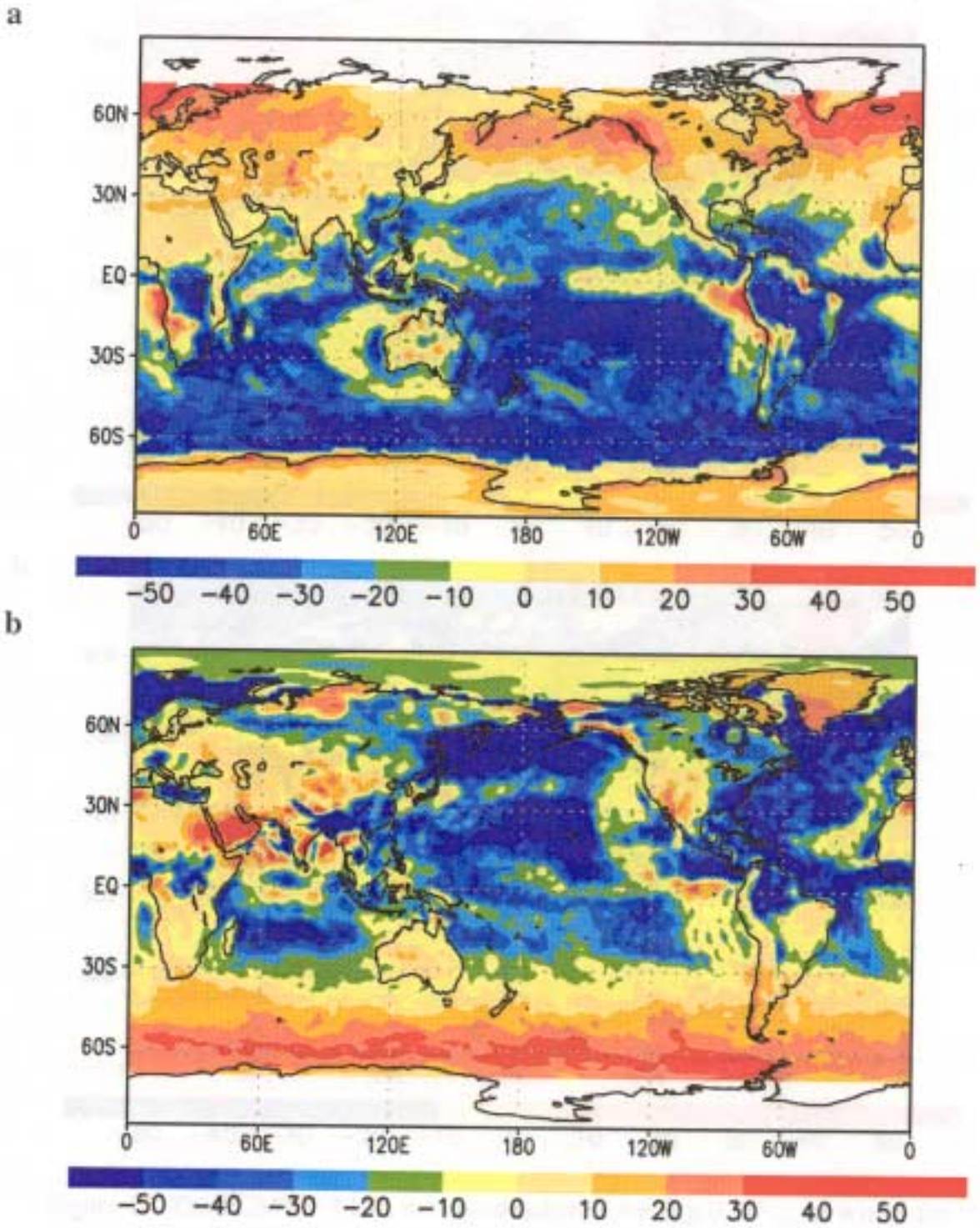

Figure 11. The ECMWF T63 net cloud radiative forcing (CRF_{net} in Wm^{-2}) for: a) January, and b) July.

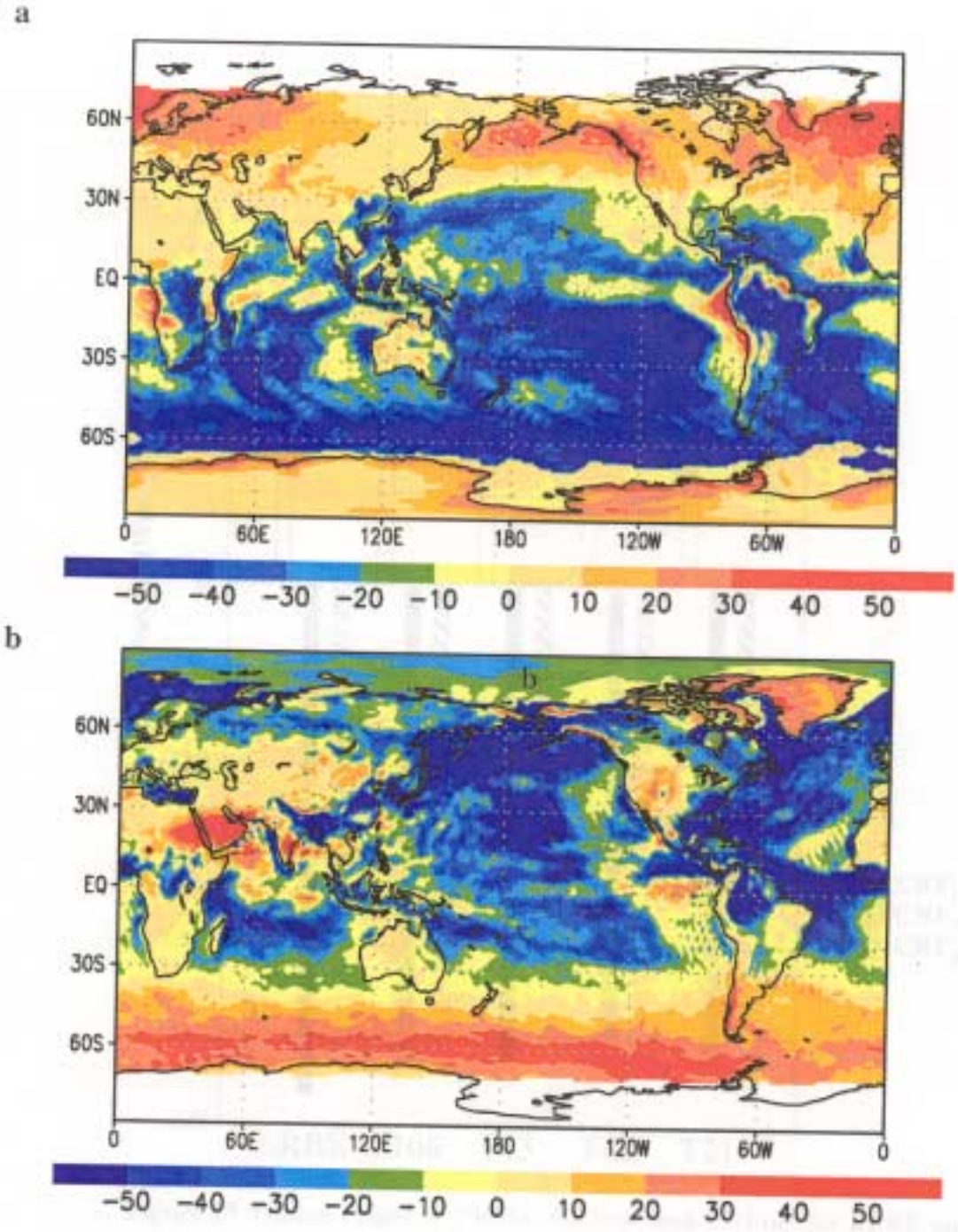

Figure 12. The ECMWF T106 net cloud radiative forcing (CRF_{net} in Wm^{-2}) for: a) January, and b) July.

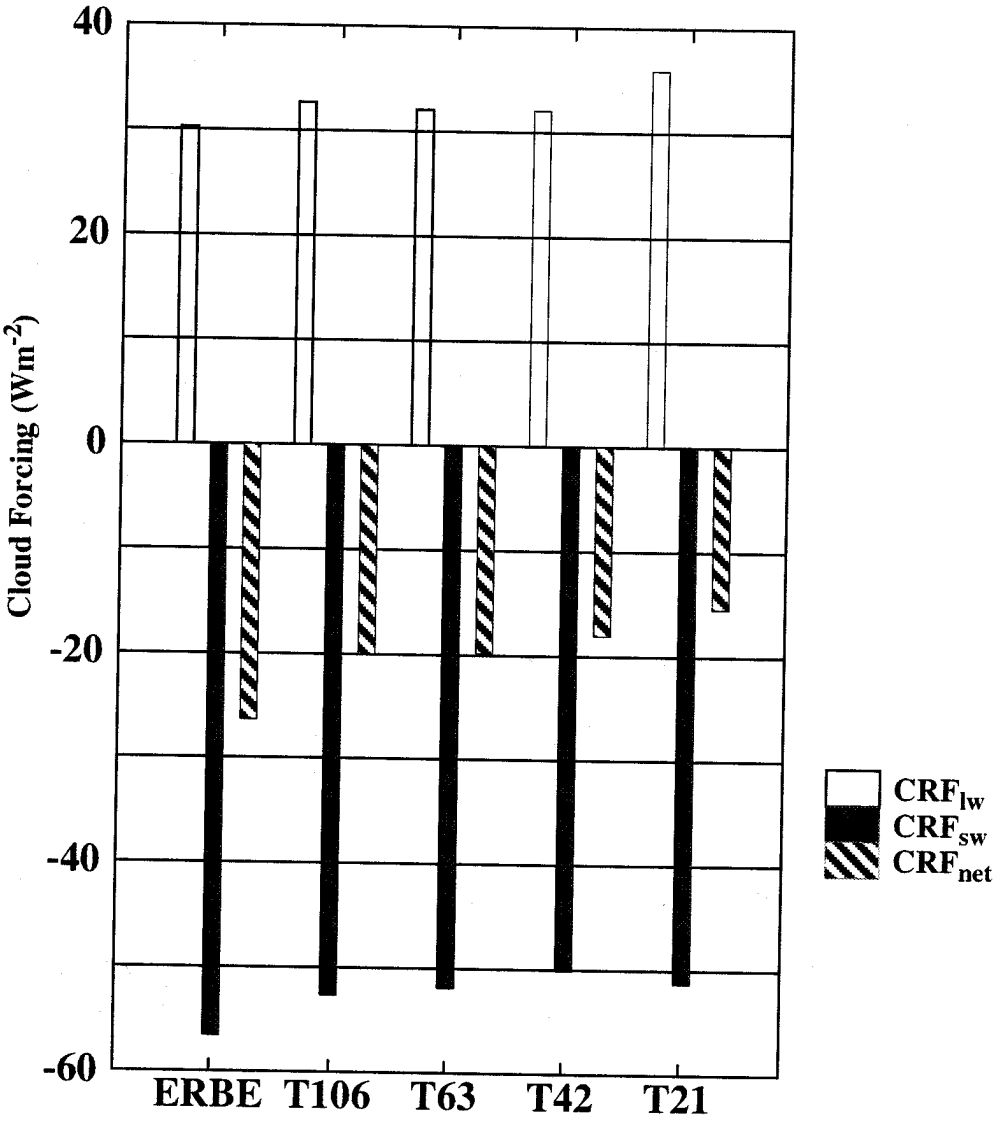

Figure 13. Global values of CRFlw, CRFsw, and CRFnet for ERBE and the ECMWF cy33 GCM (Wm^{-2}).

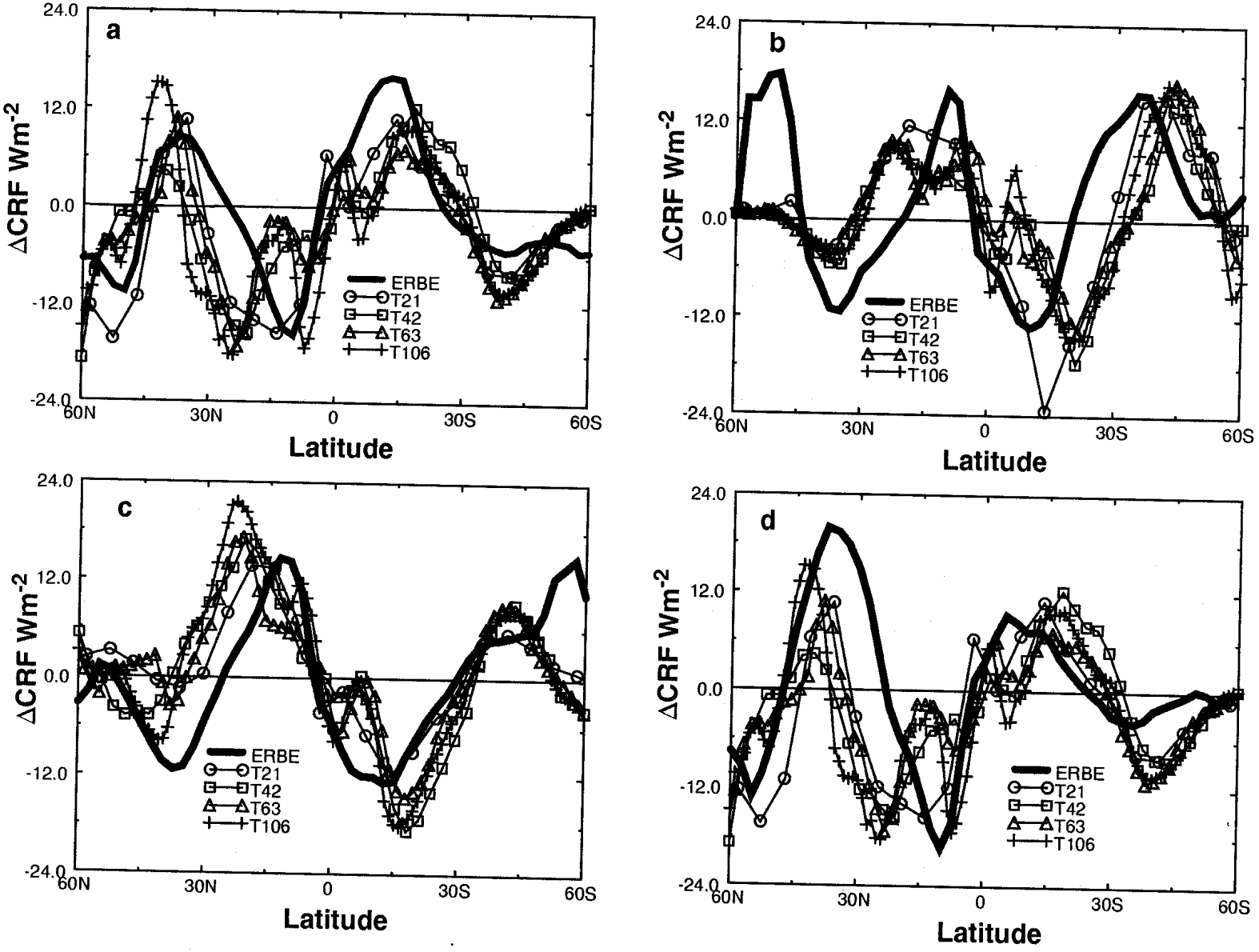

Figure 14 . Zonal average values of ΔCRF for ERBE (averaged 1985-1988) solid black line, for a) January ΔCRF_{lw}, b) January ΔCRF_{sw}, c) July ΔCRF_{lw}, and d) July ΔCRF_{sw}.

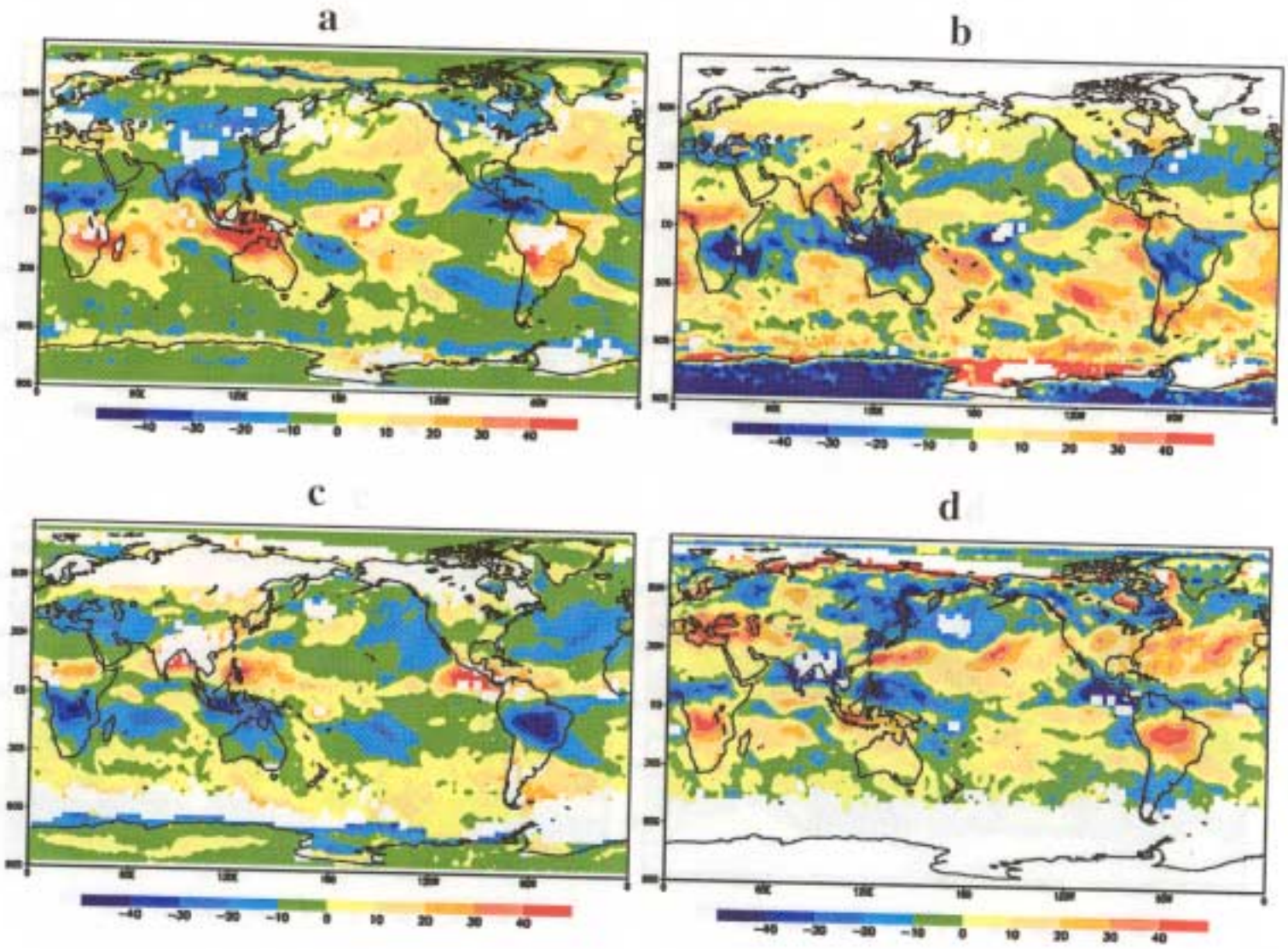

Figure 15 . The ERBE 1988 ΔCRF in Wm^{-2} for: a) January ΔCRF_{lw}, b) January ΔCRF_{sw}, c) July ΔCRF_{lw} and d) July ΔCRF_{sw}.

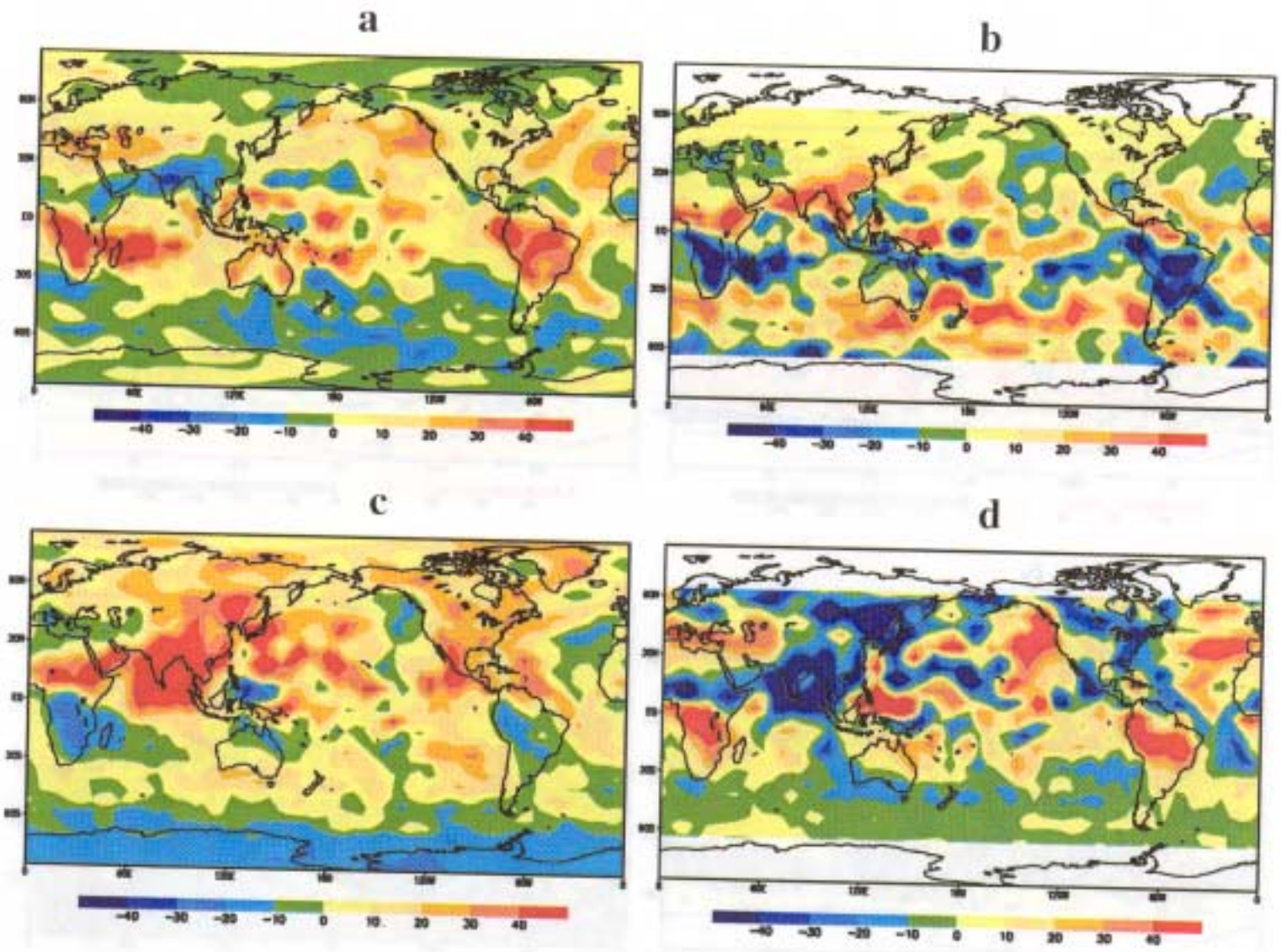

Figure 16. The ECMWF T21 resolution ΔCRF in Wm-2 for: a) January ΔCRF_{lw}, b) January ΔCRF_{sw}, c) July ΔCRF_{lw} and d) July ΔCRF_{sw}.

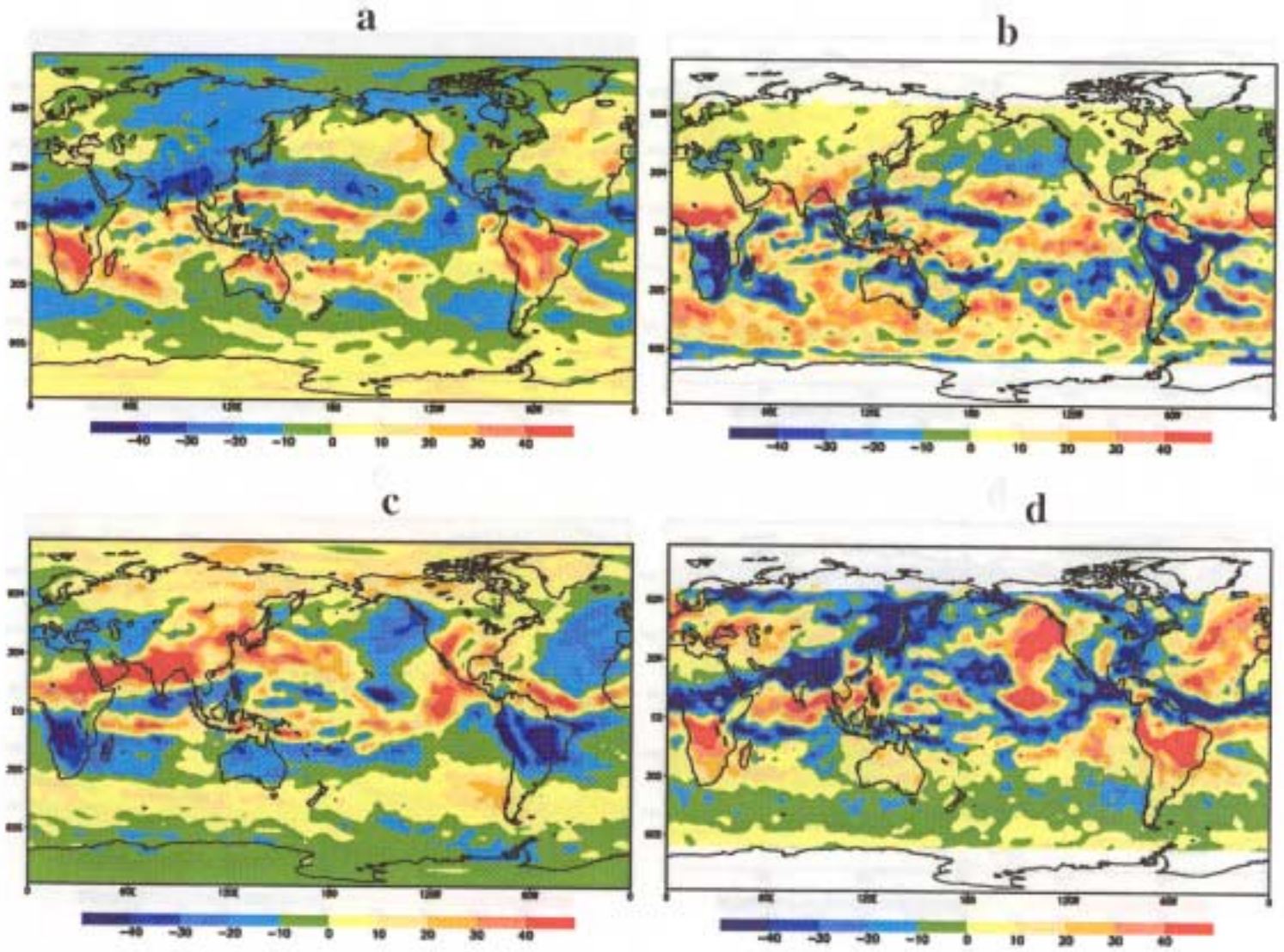

Figure 17. The ECMWF T42 resolution ΔCRF in Wm-2 for: a) January ΔCRF_{lw}, b) January ΔCRF_{sw}, c) July ΔCRF_{lw} and d) July ΔCRF_{sw}.

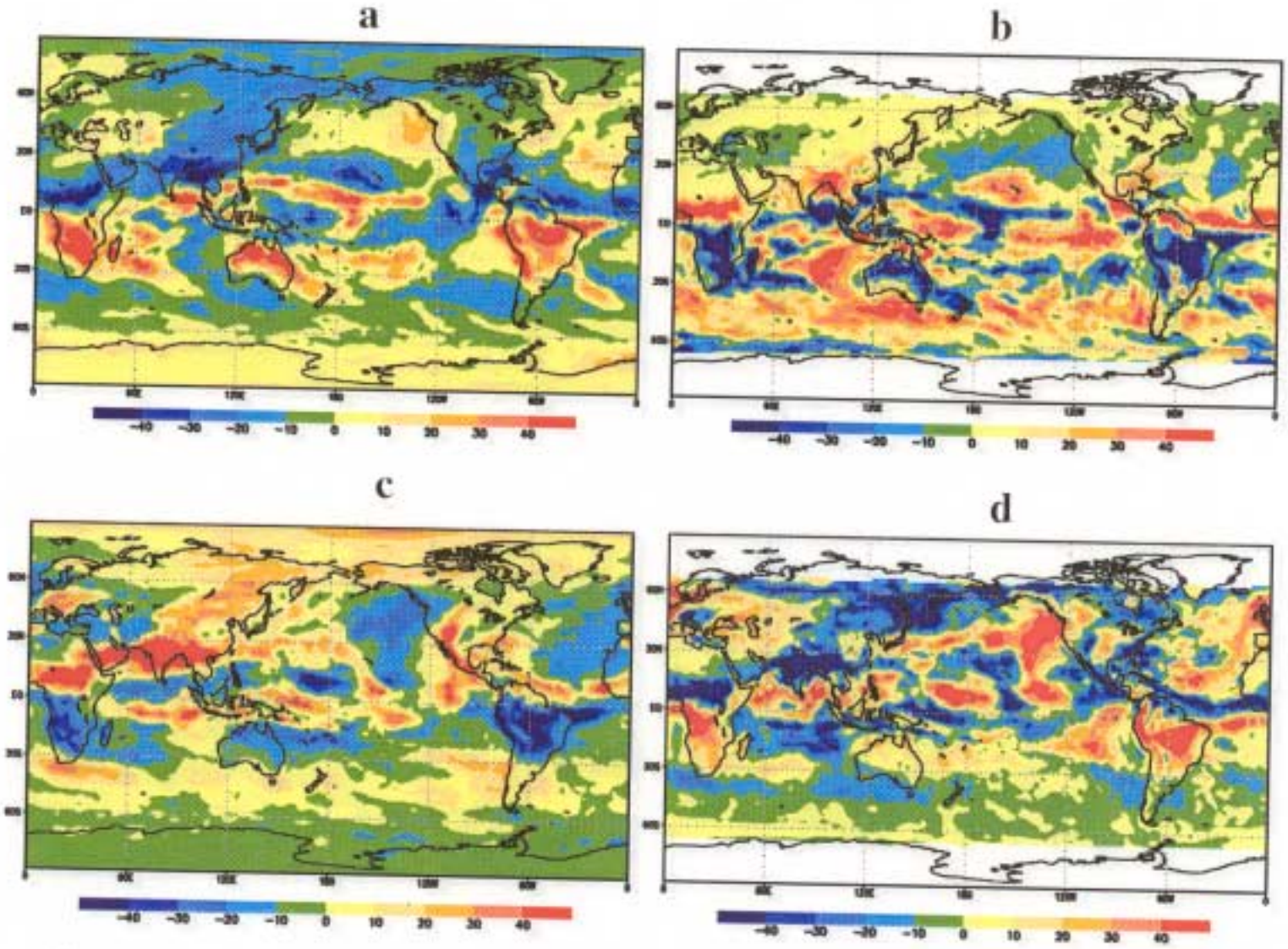

Figure 18. The ECMWF T63 resolution ΔCRF in Wm-2 for: a) January ΔCRF_{lw}, b) January ΔCRF_{sw}, c) July ΔCRF_{lw} and d) July ΔCRF_{sw}.

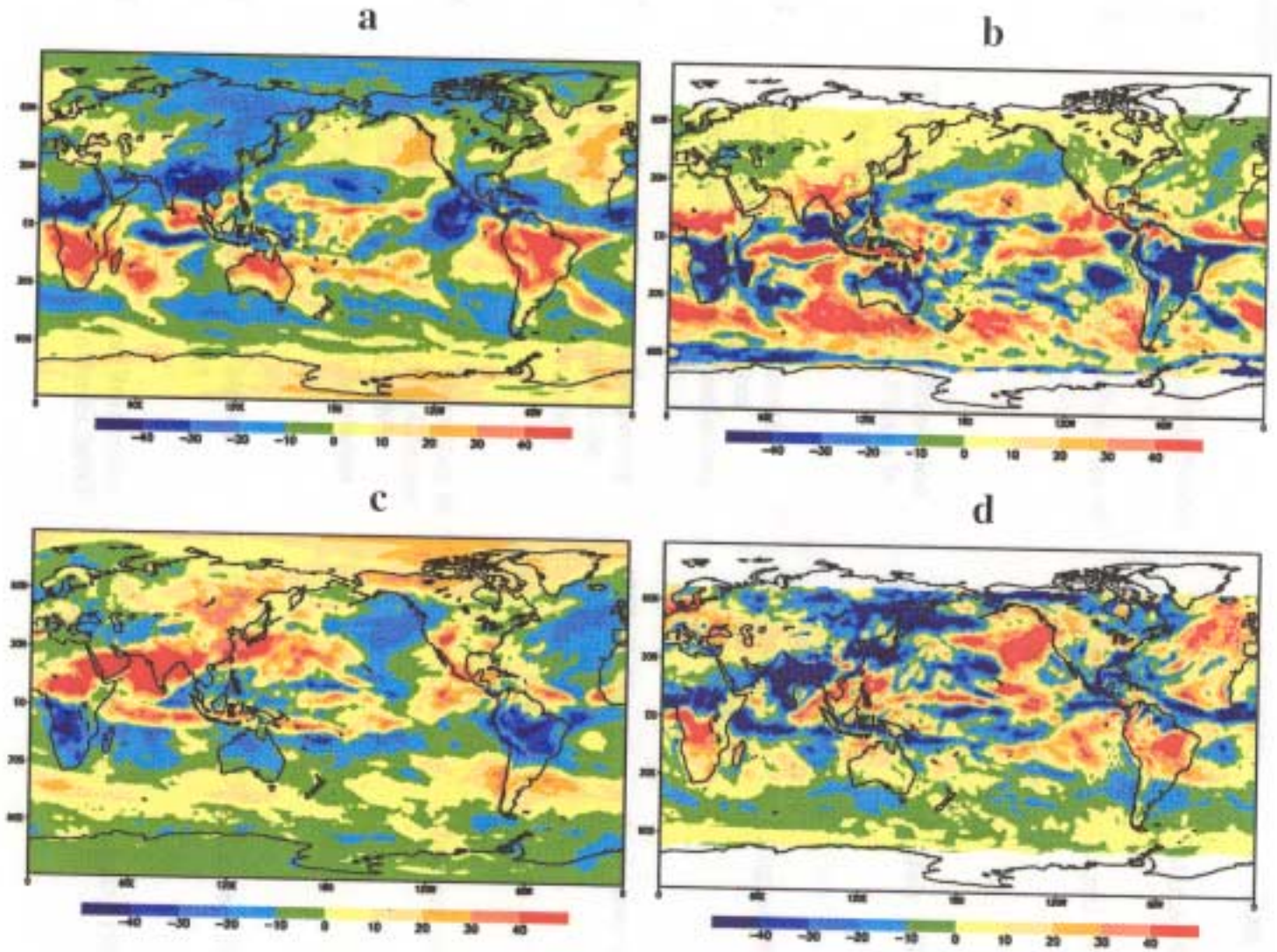

Figure 19. The ECMWF T106 resolution ΔCRF in Wm-2 for: a) January ΔCRF_{lw}, b) January ΔCRF_{sw}, c) July ΔCRF_{lw} and d) July ΔCRF_{sw}.